Journal of Materials Chemistry A

RSC Publishing

PAPER

View Article Online
View Journal | View Issue

Monochromatic visible light-driven photocatalysis realized on 2D ZnO shell arrays†

Cite this: J. Mater. Chem. A, 2013, 1, 9132

Fei Wang,[ab] Dongxu Zhao,*[a] Zhikun Xu,[ab] Zhongkui Zheng,[a] Ligong Zhang[a] and Dezhen Shen[a]

Received 2nd May 2013
Accepted 29th May 2013

DOI: 10.1039/c3ta11742a

www.rsc.org/MaterialsA

Using sunlight to solve energy shortage and pollution problems is still a hot but challenging issue. Because of this, we have demonstrated a novel and simple approach to fabricating a 2D shell array structure to enhance the interaction between incident light and the material. The enhancement remarkably increased the two-photon excitation efficiency of the material and, utilizing the two-photon induced electron–hole pairs in ZnO, we realized photocatalysis under monochromatic visible light for the first time. The method and theory described in this paper provide the basis for realizing high-efficiency sunlight-driven photocatalysts and also show a new way to improve the performance of photoelectric and photonic devices.

1 Introduction

For the increasingly severe energy shortage and environment problems, semiconductors were expected to play an important role in photocatalysis, such as in hydrogen production and pollutant degradation. Photocatalysts based on the semiconductors TiO_2 and ZnO have been successfully fabricated and widely used.[1–9] However, owing to their wide band gaps (3.2 eV for TiO_2 and 3.37 eV for ZnO), their photocatalytic applications could only be performed under ultraviolet (UV) illumination, which occupies a small part of sunlight and needs an extra UV source. In order to develop solar-driven photocatalysts without the need for extra light sources, several approaches were taken to break through this inherent restriction of the materials, such as doping to narrow the band gap,[2,3] modification by plasmonic nanoparticles to obtain light absorption in visible region,[4,5] surface hydrogenation[6] and formation of a reverse opal structure[7–9] to enhance the light harvesting. These reports did improve the photocatalytic performance of the materials under the light of a broad band from ultraviolet to visible. However, there are few reports about monochromatic visible light-driven photocatalysis, and the exact mechanism of the improvement is unclear, which are the fundamental problems that must be solved to realize high efficiency photocatalysis working under the solar light.

In this report, we used polystyrene (PS) nanospheres as a template to build ZnO 2-dimensional (2D) shell arrays. In previous work, TiO_2 3-dimensional (3D) shell arrays, or 3D photonic crystals of the reverse opal strucrure, have been fabricated,[7–9] and there is a Bragg diffraction in the lattices according to:

$$m\lambda_{\min} = 2d(n^2 - \sin^2\theta)^{1/2} \quad (1)$$

where m is the order of diffraction, λ is the wavelength of the stop band, n is the mean refraction index of the 3D crystal and d is the periodical constant along the normal of the sample plane. From the equation we can see that the stop band is very sensitive to the incident angle θ, which is a disadvantage in photocatalytic applications, but 2D shell arrays are almost θ-independent.[10] Meanwhile, the layer number of the 3D structure is more difficult to control, and the template technique using PS spheres to form 2D array structures has been reported by Li *et al.*[11–13] Furthermore, two-photon excited ZnO photoluminescence has been observed by some research groups,[14–16] which means that visible light-induced electron–hole pairs in ZnO are realizable. Considering the above points we fabricated 2D ZnO shell array structures.

2 Results and discussions

The 2D arrays of PS spheres with diameters of 200 nm, 500 nm, 750 nm and 1000 nm were fabricated. As an important characterization method of band structures, the optical transmission spectra will show us information on the stop band gaps and the changing regularity of the band gap in the different fabrication steps, which are similar to the photonic band structures of 3D photonic crystals. We show the optical transmission spectra of the samples in Fig. 1. In Fig. 1, the peaks

[a]State Key Laboratory of Luminescence and Applications, Changchun Institute of Optics, Fine Mechanics and Physics, Chinese Academy of Sciences, 3888 Dongnanhu Road, Changchun 130033, People's Republic of China. E-mail: dxzhao2000@yahoo.com.cn; Fax: +86-431-4627031; Tel: +86-431-86176322

[b]Graduate School of the Chinese Academy of Sciences, Beijing 100049, People's Republic of China

† Electronic supplementary information (ESI) available. See DOI: 10.1039/c3ta11742a

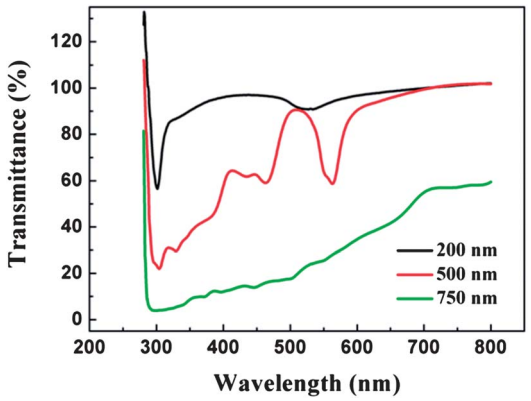

Fig. 1 The optical transmission spectra of 2D arrays consisting of 200 nm, 500 nm, 750 nm PS spheres.

located at 300 nm can be attributed to the characteristic absorption of the polystyrene material. The array of 200 nm PS spheres only has one peak located at 530 nm on the curve, and the arrays of 750 nm and 1000 nm PS spheres have complicated and unclear optical transmission spectra (the optical transmission spectra of 1000 nm PS spheres is shown in Fig. S2†). Only the 500 nm PS spheres array has a characteristic and distinct band structure in the visible light region, so we investigated it in this work. Fig. 2a and b show the FESEM images of the 500 nm sample after removing the PS spheres. The thickness of the ZnO shell is about 50 nm, and it can be seen that the ZnO shell can perfectly hold the sphere shape with the absence of the PS spheres and maintain the hexagonal array. Fig. 2c shows the optical transmission spectra of the samples. The black curve in Fig. 2c is the transmission spectrum of the 2D array self-assembled by the PS spheres. There are many characteristic peaks on the curve. The peak located at 300 nm is due to the characteristic absorption of the polystyrene material, and the 4 other major peaks are related to the positions of forbidden bands. In 3D photonic crystals, each PS sphere is regarded as a point of crystal lattices and a modified Bragg's law (eqn (1)) is widely used to calculate the photonic band gap.[6–9] However, this method has some disadvantages: it only considers the diffraction in the photonic crystal, and ignores the scattering and reflection of the PS sphere arrays. This means the result could only show one of the photonic forbidden bands and has a certain deviation from the experimental values. Herein, we have successfully simulated the accurate stop bands which fit our experimental results well.

In our 2D arrays the Bragg diffraction will no longer take effect, and light passing through the structure will only be affected by the monolayer of the PS sphere array. The dielectric spheres are efficient scatterers and the reflection of the sphere array is very limited, so the scattering by the spheres plays the dominant role in forming the band structures. According to scattering theory, when the size of the sphere is comparable to the incident light wavelength, the Rayleigh scattering model will break down, and Mie's scattering model can be used to determine the intensity of the scattered radiation. Mie's model is the exact mathematical solution of light scattering by homogeneous spheres on the basis of Maxwell's equations. For incident light of wavelength λ, the scattering behavior of a system, which consists of spherical particles, can be fully

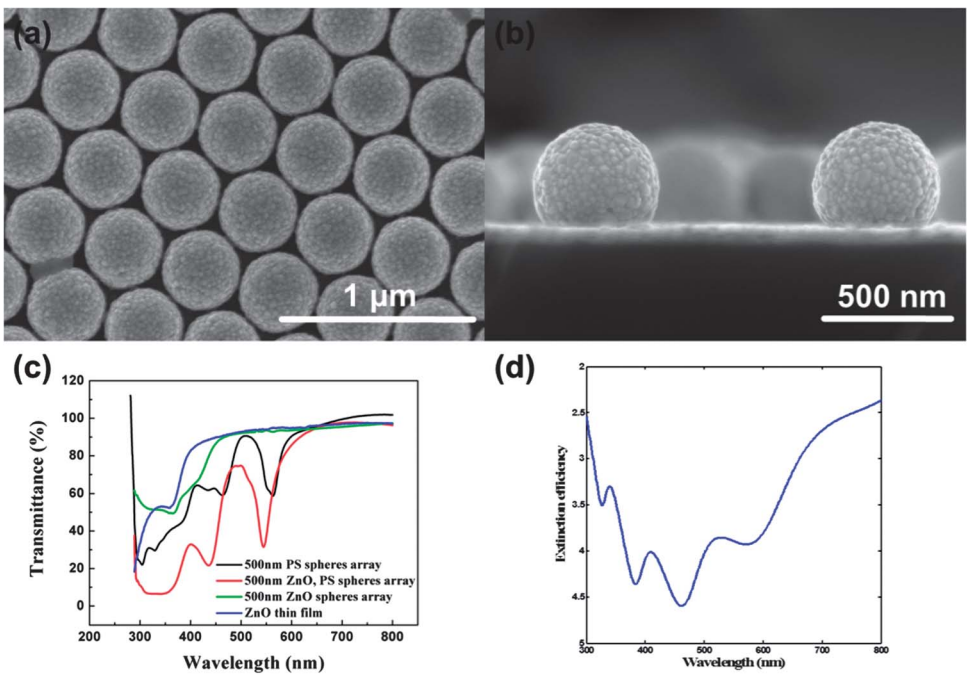

Fig. 2 (a) and (b) SEM images of the ZnO 2D shell array after removing the PS spheres. (c) Optical transmission spectra of the sample in the different formation stages. The black curve is the spectrum of the 500 nm PS sphere array. The red curve is the spectrum of the sample after coating the PS spheres with ZnO shells, and the green curve is the spectrum after removing the PS spheres from the sample. The blue curve is the transmission spectrum of ZnO thin film for comparison. (d) Simulated extinction spectrum of the 500 nm PS sphere array.

described by the particle radius r, the refractive indices, n_s and n_a, of the sphere and ambient medium respectively.[17,18] The complex Mie coefficients a_n and b_n can be calculated using complex Bessel–Riccati functions ψ and ξ:

$$a_n = \frac{\psi_n'(mx)\psi_n(x) - m\psi_n(mx)\psi_n'(x)}{\psi_n'(mx)\xi_n(x) - m\psi_n(mx)\xi_n'(x)} \quad (2)$$

$$b_n = \frac{m\psi_n'(mx)\psi_n(x) - \psi_n(mx)\psi_n'(x)}{m\psi_n'(mx)\xi_n(x) - \psi_n(mx)\xi_n'(x)} \quad (3)$$

where $m = n_s/n_a$ and is the relative refractive index of the sphere, and x is taken as

$$x = 2\pi n_a r/\lambda. \quad (4)$$

From the model we know that in a 2D array structure of PS spheres, r, n_s, and n_a are constant. However, with different incident wavelengths λ, the degrees of scattering are different, which means that for light of different wavelengths, our 2D sphere array will extinct the light that has a strong scattering intensity, and be transparent to other light with relatively weak scattering effects. This results in the band gap in our 2D PS sphere array. The scattering and extinction efficiencies are derived as:

$$Q_{Sca} = \frac{2}{x^2}\sum_{n=1}^{\infty}(2n+1)\left(|a_n|^2 + |b_n|^2\right) \quad (5)$$

$$Q_{Ext} = \frac{2}{x^2}\sum_{n=1}^{\infty}(2n+1)\mathrm{Re}(a_n + b_n). \quad (6)$$

In order to simulate the band structure of the 2D sphere array, firstly we need to know the relation between the wavelength and extinction efficiency. We treated the wavelength of the incident light as a variable, and Q_{Ext} is a function of λ. When λ increases from 300 nm to 800 nm, the extinction efficiency will change accordingly. Fig. 2d is the simulation of the extinction spectrum. Since the light transmittance is inversely proportional to the extinction efficiency, we reversed the y axis for a direct contrast. There are 4 peaks in the spectrum, located at 560 nm, 460 nm, 380 nm and 330 nm, which are in good agreement with the experimental data in Fig. 2c (black curve). Additionally, the errors between the experimental results and simulated values are less than 5 nm, which is more accurate than the errors of about 20 nm in the Bragg diffraction method. Moreover, this method can simulate the complex band structure of the sphere array, instead of only one band as in the previous method. There are also other factors which insignificantly influence the band structure, such as the diffraction and reflection of light by the sphere array. All of these factors form the final band structure of the 2D sphere array shown in Fig. 2c.

The red curve in Fig. 2c is the transmission spectrum after coating the PS spheres with ZnO. Compared with the black curve, we can see that the spectrum blue-shifted integrally, and the absorption peak at 460 nm was enhanced. Due to the rough surface of the ZnO spheres shown in Fig. 2a and b, the scattering at the surface of the spheres becomes more irregular and complicated, and the Mie scattering theory is no longer suitable for asymmetrical and non-uniform spheres. For deducing the changing regularity of the band structure, the geometrical optics theory was adopted. Because the scattering mainly occurs at the interface between the spheres and the ambient medium, we use the relative refraction index of the spheres,

$$n_r = n_s/n_a, \quad (7)$$

for the dispersion relation:

$$v = f\lambda \quad (8)$$

$$n = v_c/v. \quad (9)$$

From this we can obtain

$$v_c/f = n_r\lambda = n_s\lambda/n_a \quad (10)$$

where v_c and v are the light velocity in vacuum and medium respectively, and f is the frequency of light. v_c is constant and f depends on the light source, so v_c/f is constant. According to eqn (10), when the sphere is coated with ZnO, n_a increases from 1 to 2.45, and λ will increase, leading to a red-shift, but in the transmittance spectra, λ is the wavelength of external light, so the red-shift of λ results in the red-shift of the x-axis and the blue-shift of the curve, which explains the change of the red curve. The green curve is the spectrum of the ZnO sphere array after removing the PS spheres. On the curve, the peaks from the 2D PS sphere array have vanished, but the absorption peak located at 430 nm remains. According to eqn (10), without the PS spheres, n_s decreases from 1.579 to 1, so λ will increase again, which results in the peak located at 430 nm blue-shifting to 410 nm on the green curve. Due to the 2D structure of the ZnO hollow sphere array, we extended the transmission edge of ZnO into the visible region (the blue line is the transmission curve of ZnO thin film for comparison, and the transmittance spectra for other PS sphere conditions were shown in the ESI† and are in accord with our deductions).

Since the 2D array structures extend the transmission edge of ZnO to the visible light region, the ZnO hollow sphere array could be used as a superior photocatalyst. Methylene blue is a water contaminant from dyeing processes, and the visible light-driven photocatalytic activity of the shell array was measured by monitoring the change of the optical absorption of the methylene blue solution. According to the band gaps of the green curve in Fig. 2c, monochromatic visible light centered at 400 nm and 470 nm was used in the experiment. The ZnO shell array used as the photocatalyst was cut into 0.5 cm × 0.5 cm size, and the ZnO thin film used for comparison was 1.0 cm × 1.0 cm, so we can ignore the surface area difference of the ZnO material. The photocatalytic degradation is shown in Fig. 3a. From Fig. 3a we can see that under the illumination of 400 nm light (2 mW cm^{-2}), the absorption peak of the methylene blue decreased, which means that the decomposition of methylene blue has indeed taken place. However, as shown in Fig. 3b, the photocatalysis reaction did not occur under 470 nm light (4 mW cm^{-2}), which is the high transparent region in the band gap (shown in Fig. 2c). In

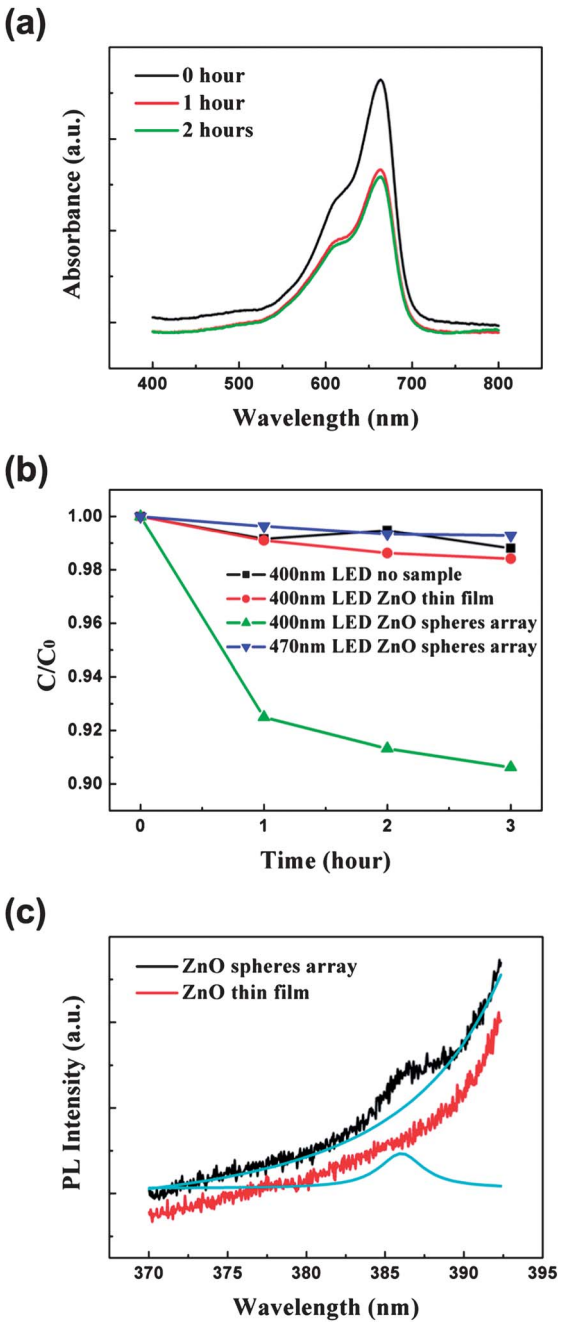

Fig. 3 (a) The optical absorption of the methylene blue solution after different degradation times. (b) The photocatalytic activity of the sample under different reaction conditions. (c) The room temperature PL spectra of the ZnO thin film and ZnO 2D sphere array after removing the PS spheres. The cyan curves are the Gaussian fitting results of the black curve.

addition, for the ZnO thin film without the 2D array structure, no reaction was observed. From the above experiment we can infer that the 2D shell array structure of ZnO plays an important role in the visible light-driven photocatalysis.

The photocatalysis may caused by two-photon excitation in ZnO.[14–16] For a photon with energy less than the band gap of the material, the hole–electron pairs can not be generated in the material. But, if an electron in the valence band of ZnO absorbs more than two photons, it will transit to a higher state in the conduction band, and generate a hole in the valence band at the same time. This electron–hole pair will assist in oxidizing absorbed organic pollutants.[19] For the wavelength in the band, the incident light strongly scatters at the surface of the ZnO hollow spheres and the interface between the ZnO shell and the air core. The scattered light then transfers to neighboring spheres and will be scattered or absorbed by the neighboring sphere, which causes a strong resonant mode among the spheres in the array.[20–22] Furthermore, the velocity of electromagnetic pulse propagation is determined by the group velocity v_g, where

$$v_g = \frac{\partial \omega}{\partial \kappa} = c\left(n + \omega \frac{dn}{d\omega}\right)^{-1}. \quad (11)$$

In photonic crystals, the slope of the bands, $\omega(k)$, decreases when approaching the band edges, that is, the derivative of $\omega(k)$ tends to zero. This means that the group velocity is considerably reduced when approaching band gaps.[23–27] Both the resonant mode and the slow photon effect will drastically enhance the interactions between light and matter, and increase the chances of two-photon excitation.

In order to further prove the two-photon excitation process in the ZnO 2D shell array, up-conversion photoluminescence measurements were performed by using a frequency-doubled femtosecond laser with a wavelength of 400 nm as the excitation source. Fig. 3c shows the room-temperature photoluminescence spectra. A near-band-edge emission peak of ZnO located at 385 nm is observed in the array structure, but no emission peak was observed for the ZnO thin film. This experiment supports our opinion that the 2D shell array structure of ZnO can increase the two-photon excitation efficiency. However, when the wavelength of the incident light is not located in the range of the band gap, the crystal is almost transparent to the light. This is why the array of ZnO spheres did not work under 470 nm illumination, as presented in Fig. 3b.

It is worth noting that the sample still containing the PS spheres has a strong absorption peak located at about 430 nm on the red curve in Fig. 2c, which results from the combination of the band gaps of the ZnO spherical shell array and the inner PS spheres. Will the ZnO hollow spheres together with inner PS spheres have stronger resonance and slow photon effects? To confirm this, their photocatalytic capability was evaluated and shown in Fig. 4a. When under the illumination of 430 nm light (0.5 mW cm^{-2}), the sample presented good photocatalytic performance. We used the degradation rate constant κ to compare the photocatalytic activity of the samples with and without PS spheres. From Fig. 4b we can see that the photocatalytic process of the ZnO sphere array tends to slow down obviously after the reaction time of an hour, but the 2D array containing the PS spheres still has a fast degradation rate even when driven by a low power density light of 0.5 mW cm^{-2}. According to the mechanism of photocatalysis,[28] the excited photocatalysts can only decompose the organic species absorbed on the surface. We now take the absorbing velocity v_{ab} and degradation velocity v_{de} into consideration. With a certain absorbing velocity v_{ab}, the slowing of the photocatalytic process in the ZnO sphere array indicates that the photocatalysts can

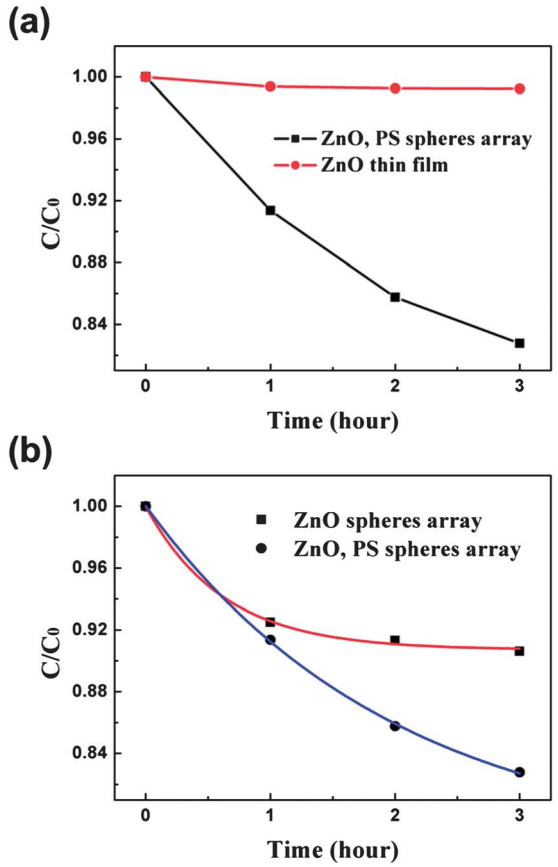

Fig. 4 (a) The photocatalytic activity of the sample containing the PS spheres. (b) The degradation rate constant of the samples without the PS spheres and containing the PS spheres.

not degrade all of the absorbed organic pollutants, and the excessive organic species on the surface isolated the photocatalysts from the solution, corresponding to $\nu_{de} < \nu_{ab}$. The excited electron–hole pairs are low in number. However, for the 2D array containing the PS spheres, the degradation rate is maintained even after 3 hours, meaning the degradation velocity of the sample must be faster than the absorbing velocity, so $\nu_{de} \geq \nu_{ab}$. This means more electron–hole pairs are induced due to the high two-photon excitation efficiency. Therefore we can infer that due to the combined deeper dip in the transmittance spectrum, the photonic effects caused by the PS sphere array could also act on ZnO. The ZnO spherical shell array, together with the inner PS spheres, has stronger photonic effects and leads to a higher excitation efficiency, which confirms that the photocatalysis of our samples is the result of photonic effects, and stronger effects will result in superior photocatalytic properties.

3 Conclusions

In summary, 2D shell arrays of ZnO were successfully fabricated by a simple PS microsphere-assisted templating technique. The band gaps of the array structure were investigated by the optical transmission spectra. According to Mie's scattering theory, we accurately deduced the band structure and changing regularity that fit the experimental results well. The photocatalytic capability of the crystals was evaluated by the photocatalytic degradation of methylene blue, and we realized monochromatic visible-light driven photocatalysis by two-photon excited electron–hole pairs in ZnO. It was proved that the 2D array structures could change and enhance the performance of optoelectronic devices based on semiconductors. This work not only shows a way to achieve high-efficiency, sunlight-driven photocatalysis to solve environmental and energy problems, but also provides a new method to improve the properties of photoelectric and photonic devices in the future.

4 Experimental

Glass substrates were cut into 1 cm × 1 cm pieces, and ultrasonically cleaned in acetone, ethanol and deionized water separately, each for 15 minutes. Subsequently, the substrates were placed in a solution of 7% NH_4OH, 30% H_2O_2, and deionized water (1 : 1 : 5) by volume for 60 minutes at 80 °C, then rinsed in deionized water and dried at room temperature. Polystyrene sphere suspensions (200 nm, 500 nm, 750 nm, 1000 nm in diameter, purchased from Alfa Aesar corporation and used as received) were spin-coated on the glass, and then heated at 90 °C to make the PS spheres melt slightly and stick to the substrates. ZnO was deposited onto the samples by a radio-frequency magnetron sputtering technique with a deposition time of 30 minutes. To coat the microspheres with ZnO wholly and uniformly, we tilted the sputtering source of ZnO at a certain angle to the sample holder, and rotated the sample holder with a speed of 20 r min^{-1}. Finally, we immersed the samples in toluene for 5 minutes and annealed them at 400 °C for 30 min to entirely remove the PS. The samples used for comparison were fabricated by the same method but without coating the PS spheres onto the substrates. The ZnO shell and thin film were about 50 nm thick, and the thickness of ZnO will not affect the band structures of our samples.

The photocatalytic activities of the samples were evaluated by the degradation of methylene blue aqueous solution (1 μM) in a quartz cuvette in a darkroom. The monochromator (Shimadzu RF-520) equipped with a 150 W Xe lamp and commercial LEDs (400 nm, 450 nm) served as the visible light sources. The UV-vis absorption spectra of the substrates as a function of time were recorded. The morphology of the samples was investigated by field-emission scanning electron microscopy (FESEM, Hitachi S-4800), and the absorption spectra were carried out using a Shimadzu UV-3101 PC spectrophotometer. When testing, we used a glass substrate as a reference. The photoluminescence (PL) measurements were performed using a frequency-doubled femtosecond laser with a wavelength of 400 nm as the excitation source. The power densities of driven light were measured by an Ophir PD300R-UV power meter.

Acknowledgements

This work is supported by the National Basic Research Program of China (973 Program) under Grant no. 2011CB302006, 2011CB302004, and the Knowledge Innovation Program of the Chinese Academy of Sciences under Grant no. KJCX2-YW-W25.

Notes and references

1 J. L. Yang, S. J. An, W. I. Park, G. C. Yi and W. Choi, *Adv. Mater*, 2004, **16**, 1661.
2 R. Asahi, T. Morikawa, T. Ohwaki, K. Aoki and Y. Taga, *Science*, 2001, **293**, 269.
3 W. Y. Su, Y. F. Zhang, Z. H. Li, L. Wu, X. X. Wang, J. Q. Li and X. Z. Fu, *Langmuir*, 2008, **24**, 3422.
4 Y. Lu, H. T. Yu, S. Chen, X. Quan and H. M. Zhao, *Environ. Sci. Technol.*, 2012, **46**, 1724.
5 Y. H. Zheng, L. R. Zheng, Y. Y. Zhan, X. Y. Lin, Q. Zheng and K. M. Wei, *Inorg. Chem.*, 2007, **46**, 6980.
6 X. B. Chen, L. Liu, Y. P. Yu and S. S. Mao, *Science*, 2011, **331**, 746.
7 M. Wu, Y. Li, Z. Deng and B. L. Su, *ChemSusChem*, 2011, **4**, 1481.
8 G. Z. Liao, S. Chen, X. Quan, H. Chen and Y. B. Zhang, *Environ. Sci. Technol.*, 2010, **44**, 3481.
9 M. M. Ren, R. Ravikrishna and K. T. Valsaraj, *Environ. Sci. Technol.*, 2006, **40**, 7029.
10 G. T. Duan, W. P. Cai, Y. Y. Luo and F. Q. Sun, *Adv. Funct. Mater.*, 2007, **17**, 644.
11 Y. Li, N. Koshizaki, H. Wang and Y. Shimizu, *ACS Nano*, 2011, **5**, 9403.
12 Y. Li, N. Koshizaki, Y. Shimizu, L. Li, S. Gao and T. Sasaki, *ACS Appl. Mater. Interfaces*, 2009, **1**, 2580.
13 Y. Li, G. Duan, G. Liu and W. Cai, *Chem. Soc. Rev.*, 2013, **42**, 3614.
14 J. H. Lin, Y. J. Chen, H. Y. Lin and W. F. Hsieh, *J. Appl. Phys.*, 2005, **97**, 033526.
15 C. F. Zhang, G. J. Dong, G. J. You and S. X. Qian, *Appl. Phys. Lett.*, 2005, **87**, 051920.
16 E. V. Chelnokov, N. Bityurin, I. Ozerov and W. Marine, *Appl. Phys. Lett.*, 2006, **89**, 171119.
17 H. C. Hulst, *Light Scattering by Small Particles*, Dover, New York, 1981.
18 S. M. Scholz, R. Vacassy, J. Dutta, H. Hofmann and M. Akinc, *J. Appl. Phys.*, 1998, **83**, 7860.
19 S. R. Morrison and T. Freund, *J. Chem. Phys.*, 1967, **47**, 1543.
20 R. F. Pasternack and P. J. Collings, *Science*, 1995, **269**, 935.
21 H. Xu, X. Q. Chen, S. Ouyang, T. Kako and J. H. Ye, *J. Phys. Chem. C*, 2012, **116**, 3833.
22 S. Gottardo, R. Sapienza, P. D. Garcia, A. Blanco, D. S. Wiersma and C. Lopez, *Nat. Photonics*, 2008, **2**, 429.
23 A. Imhof, W. L. Vos, R. Sprik and A. Lagendijk, *Phys. Rev. Lett.*, 1999, **83**, 2942.
24 J. I. L. Chen, G. V. Freymann, S. Y. Choi, V. Kitaev and G. A. Ozin, *Adv. Mater.*, 2006, **18**, 1915.
25 T. Baba, *Nat. Photonics*, 2008, **2**, 465.
26 B. Corcoran, C. Monat, C. Grillet, D. J. Moss, B. J. Eggleton, T. P. White, L. O'Faolain and T. F. Krauss, *Nat. Photonics*, 2009, **3**, 206.
27 P. Dardano, M. Gagliardi, I. Rendina, S. Cabrini and V. Mocella, *Light: Sci. Appl.*, 2012, **1**, e42.
28 A. L. Linsebigler, G. Lu and J. T. Yates, *Chem. Rev.*, 1995, **95**, 735.